Lasers in Manufacturing Conference 2019

Pure vanadium insert for efficient joining of Ti6Al4V to 316L stainless steel with continuous Yb:YAG laser

A. Mannucci[a,b], I. Tomashchuk[a*], A. Mathieu[a], R. Bolot[a], E. Cicala[a],

S. Lafaye[b], C. Roudeix[b]

[a]*Laboratoire Interdisciplinaire Carnot de Bourgogne, UMR CNRS-6303, Université de Bourgogne-Franche Comté, 12 rue de la Fonderie, 71200 Le Creusot, France*

[b]*SME Laser Rhône-Alpes, 49-51 Boulevard Paul Langevin, 38600 Fontaine, France*

Abstract

Laser welding of titanium alloys to stainless steels remains challenging due to the formation of brittle intermetallic compounds. Pure vanadium has full metallurgical compatibility with titanium and good solubility in iron, except the region of sigma phase, which precipitation is avoidable by rapid cooling. This makes vanadium an attractive interlayer material capable to enhance weld strength and ductility.

In the present study, the continuous double pass welding of 1 mm thick Ti6Al4V alloy and 316L steel through 2 mm wide pure vanadium insert was studied. It was found that the composition of the melted zone between steel and vanadium is a key factor determining the strength and fracture mode of the joint. In spite of absence of sigma phase, the melted zones having >40wt% V showed brittle behavior, when the presence of <40wt% V led to ductile fracture in unmelted vanadium insert. Best results of tensile strength reached 500 MPa.

Keywords: dissimilar welding; vanadium; titanium; steel

1. Introduction

Titanium and its alloys have attractive properties such as high corrosion resistance, biocompatibility, and high strength combined with a low density. These properties are useful respectively for chemical, medical and aeronautical industries, but titanium is approximately ten time more expensive than stainless steel. Their assembly will be interesting for structure improvement without excessive cost. Nevertheless, it remains challenging due to a mismatch of thermal expansion coefficient (Table 1) and the formation of brittle intermetallic compounds (Ivanchenko and Pryadko 2008). It is possible to reduce their formation to micrometric layers, situated at the limit of melted zone, when applying a sufficient beam offset from the

* Corresponding author. Tel.: +33-385-751-123 ;
E-mail address: iryna.tomashchuk@u-bourgogne.fr.

joint line (Mannucci et al. 2018). Nevertheless, the tensile behavior remains brittle, and the resulting average UTS is quite low (150 MPa).

Solid-state methods such as explosion welding (Gloc et al., 2016, Chu et al., 2017a), friction (Dey et al., 2009, Kimura et al., 2016) or friction stir welding (Fazel-Najafabadi et al., 2010, Liao et al., 2010, Ishida et al., 2015) can produce resistant joints. It is due to the interface deformation and the thickness of intermetallic rich layers, inferior to 1 µm. However, these methods are not applicable for all joining geometries.

Another solution is avoiding the mixing between titanium and stainless steel by adding an interlayer material. Very few metals are compatible simultaneously with titanium and iron. In consequence, interlayers are often only compatible with one of the base metals. Interlayers are accepted if they create the phases less brittle than these of Ti-Fe system. Tomashchuk and Sallamand, 2018, have listed the use of V, Nb, Ta, Mg, Cu, Ni and several studies with multiple inserts.

Vanadium is fully compatible with titanium, but a brittle σ phase exists between iron and titanium, in a range of 650 - 1219 °C, and between approximately 20 and 80 at.% of V, according to phase diagram given in Lyakishev, 1997. This phase has a low kinetic of formation and it may not appear with the rapid cooling proper to laser welding (Ustinovshikov et al., 2005, Tomashchuk et al. 2015). It is important to note that welding with interlayer in one step with laser spot centered at the middle of the insert did not allow avoid the formation of FeTi and Fe_2Ti intermetallics (Tomashchuk et al. 2015, Adomako et al. 2018). Chu et al., 2017b, also observed Fe-Ti intermetallics in a TIG joint between two bimetallic plates of Q235 stainless steel and pure Ti with V filler wire.

Nogami et al., 2013, and Adomako et al., 2019, studied post weld heat treatment of Fe/V assemblies. They both observed important precipitation of σ-(Fe, V) with hardness up to 1000 HV in the melted zone, where vanadium content was comprised between 20 and 80 at.%. In laser welding, Adomako et al., 2019, obtained brittle fractures with lower UTS after post weld heat treatment. In some electron beam welded samples of Nogami et al., 2013, intermetallic layers appeared after heat treatment, as well as precipitation of Ni_2V_3 and NiV_3.

The mismatch of physical properties does not cause difficulty in Ti-V-Fe joining, since V boiling and melting points are near to those of Ti and its alloys (Table 1). The thermal expansion coefficient of V and Ti are about the half of that of 316L stainless steel.

The goal of this study was to compare the effect of two different spot diameters on Ti-6Al-4V/V/316L welding, and to verify if a joint coefficient of 100 % is obtainable with decreasing global heat input. Vanadium being the weakest of the three materials, it is supposed that if fracture does not occurred in melted zones, its annealing decreases the global UTS. The vanadium content effect on hardness and microstructure of melted zones was also investigated.

Table 1. Physical properties of materials

Properties	Units	316L	T40	Ti-6Al-4V	V
Melting point / solidus	K	1663	1941	1877	2163
liquidus		1713		1933	
Boiling point	K	3013	3560	3560	3653
Thermal diffusivity	mm^2/s	3,8	9,4	2,9	10
Thermal expansion	$10^{-6}\ K^{-1}$	16,5	8,4	8,6	8,3
Density	kg/m^3	7980	4510	4430	6100
Ultimate tensile strength	MPa	590	345	1000	500
Yield strength	MPa	300	276	975	420

2. Experimental

2.1. Materials

The welding experiments were made with 150 × 50 × 1 mm plates of Ti-6Al-4V titanium alloy and 316L stainless steel. Ti-6Al-4V, provided by VSMPO-AVISMA Corporation, was annealed at 790 °C during 1h, and air-cooled. 316L stainless steel, provided by Outkumpu, was annealed at 1070 °C. Ti-6Al-4V and 316L compositions are provided in Table 2. 2 and 6 mm wide and 150 mm long vanadium inserts were laser cut from 1mm thick 99.8 % pure laminated vanadium plates provided by GoodFellow. The edges were grinded up to 600.

Table 2. Base metals composition in mass %.

Ti-6Al-4V	Ti	Al	V	Fe	C	N	H	O		
	remainder	6.21	3.99	0.13	0.025	0.003	0.003	0.13		
316L	Fe	C	Si	Mn	P	S	Cr	Ni	Mo	N
	remainder	0.023	0.49	0.90	0.035	<0.001	16.8	10.1	2.03	0.040

2.2. Welding experiment

Before welding, the three metals were cleaned with acetone; metal plates were maintained together by 5 spot welds for each assembly. Continuous laser source TruDisk 6001 (Trumpf) of 6 kW was used. The laser spot was focused on the top surface. The top and the bottom faces were protected by argon flow of 20 and 10 l/min respectively. In a preliminary experiment, metal plates were weld with a 200 µm spot, and different linear energies (Table 3 a). On each assembly, the laser spot was focused at a variable distance from the interface between V and stainless steel or Ti-6Al-4V. This beam offset (Δ) variated from 0 to a certain value (100 or 200 µm). The welding parameters were the same on Ti-6Al-4V side and on 316L side, as schematized on Fig.1. A second experiment was made in order to decrease the lineic energy of welding, and vanadium annealing, by using a 100 µm laser spot, that allows highest energy density. Ti-6Al-4V plates were weld to 2 mm large V inserts with lineic energy of 6.8 J/mm. First, a beam offset of 100 µm to Ti-6Al-4V side was applied, for b1 to b3 samples, and there were no offset for other samples. The lineic energies and beam offset applied to weld the 316L plates are described in Table 3 b.

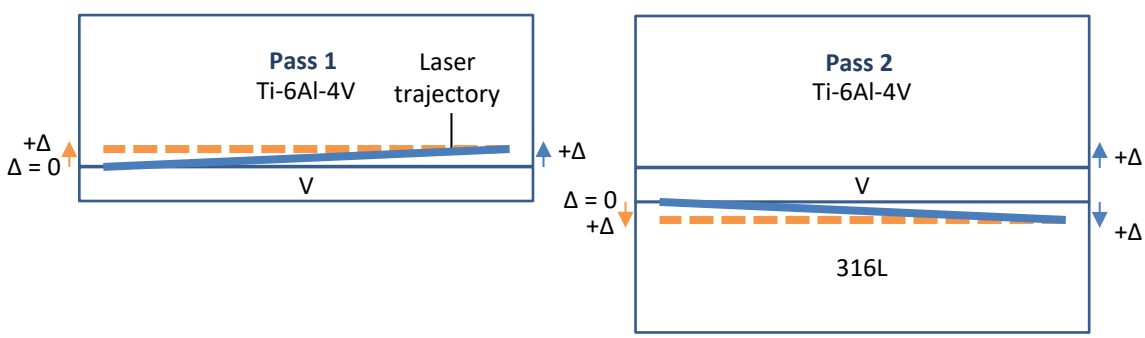

Fig.1. Schema of welding experiments. 200 µm spot welding line is represented by continuous lines, starting from Δ = 0 to +Δ, where +Δ is the same between pass 1 and pass 2. 100 µm welding line is represented by dashed lines, at constant Δ on a pass, but with different Δ between pass 1 and 2.

Table 3. Lineic energy and beam offset for a) the 200 µm spot welding, b) the 100 µm spot experiment.

(a) 200 µm spot

Sample	Lineic energy (J/mm)	Δ_{max} (µm)	V width (mm)	$\overline{UTS}$ (MPa)
a.1	18	200	6	347
a.2	18	-200	6	319
a.3	42	200	6	367
a.4	18	100	2	395
a.7	12	100	2	409
a.8	18	100	2	341

(b) 100 µm spot

Sample	Lineic energy (J/mm)	Δ (µm)	$\overline{UTS}$ (MPa)
b.1	10	-50	343
b.2	7.9	-50	374
b.3	6.5	0	412
b.4	10	0	487
b.5	7.9	0	467
b.6	10	50	494
b.7	7.9	50	477
b.8	10	100	412
b.9	7.9	100	399

2.3. Characterization

Assemblies were cut in 20 mm large strips for tensile tests and fractography study (3 samples per condition). Elemental analysis and microhardness measurements were done on cross section samples. These samples were embedded in conductive resin, grinded and polished up to colloidal silica.

Global observations and fracture analysis were made using a scanning electronic microscope JSM-6610LA (Jeol), equipped with an EDS analyzer. XRD analysis were made with PANalytical X'Pert PRO, using a Co target. The step scan was 0.0167°. For the fracture in V/316L melted zone, the scanning range was of 40−120° with counting time of 200 s per step (Fig. 10 a). For the fracture in Ti-6Al-4V/V melted zone, the scanning range was of 30-120° with counting time of 1500 s per step (Fig. 10 b). Microhardness tests were made with a Buehler device, with a 25 g charge during 10 s. Tensile tests were made with MTS Insight 30 kN tensile test machine, at cross head speed of 5 mm/min.

3. Results and discussion

3.1. Global observation and microstructure

Two pass welding resulted in formation of Ti-6Al-4V/V (MZ_{Ti}) and 316L/V (MZ_{316L}) melted zones separated by unmelted vanadium. Both melted zones have a shape typical for laser welding, with the enlargement at top and bottom. For welds performed with 100 and 200 µm spot, both top and bottom widths are similar because they are controlled mainly by convection phenomena (Marangoni convection and drag force of vapor plume), and increase with linear energy (Table 4). Above 42 J/mm with 2 mm large V, the two convection zones seem attached. Middle widths are about 2 times thinner for 100 µm spot welds, and increase proportionally to linear energy. Δ had not noticeable influence on widths.

Because V has highest thermal diffusivity and higher melting point (Table 1), it melted less than base metals, resulting in sharper interface at the limit of the melted zones.

The heat-affected zone (HAZ) of the Ti-6Al-4V (Fig. 2 a) is characterized by brighter matrix and more diffuse V-rich inclusions. Typical microstructure of HAZ is illustrated on Fig. 2 b: in solid Ti-6Al-4V bright V rich

particles diffused in the dark matrix, filled with thin martensitic needles. These martensitic needles appeared also in MZ at Ti-6Al-4V side, as shown in Fig. 2 c.

The convection in the melted zone was insufficient to homogenize totally the local composition (Fig. 3). For low V content, the MZ have homogeneous composition. For high V content, they become more heterogeneous. No reactive layer was present at any limit of melted zones.

Some pores occurred in the MZ, principally in MZ_{Ti}. Rare micro-cracks appeared in MZ_{316L} containing around 55 at.% V (in Fig. 4 a and Fig. 2 c), welded with low speed, 100 µm spot and offset of 50 µm toward V. Adomako et al., 2019 observed a small inclusion of σ-(Fe, V) phase in a pore, despite of the high cooling speed. This inclusion was detectable only with EBSD analysis, but not with XRD. They supposed the σ phase germinated at the center of the weld, because it remains at high temperature for longer time, and was the origin of the cracks: same mechanism is possible in our case, and should be confirmed by EBSD analysis.

The colloidal silica revealed the grains of stainless steel and MZ_{316L}. In agreement with the results of Adomako et al., 2019, two kinds of grains were observed in V/steel welds (Fig. 4): coarse grains in V-rich MZ, and columnar grains, growing perpendicularly to MZ interface, in V-poor MZ. If the two different microstructures are present in the same MZ, they are clearly separated: coarse grains are situated at V side, and thin columnar cells are at the 316L side. The proportion between them depends on global vanadium content (Fig. 4). Columnar solidification disappears in melted zones containing more than 40 at.% V, while for less than 10 at.% V, there is no coarse grain. Therefore, the separation between them in a MZ does not depend on the local composition, but possibly on different cooling rates of opposite extremities of the weld.

Table 4. Typical MZ widths compared for the two spot sizes.

Spot diameter (µm)	200	100
Top width (µm)	430 – 715	410 – 675
Middle width (µm)	475 – 740	215 – 270
Bottom width (µm)	310 – 380	285 – 450

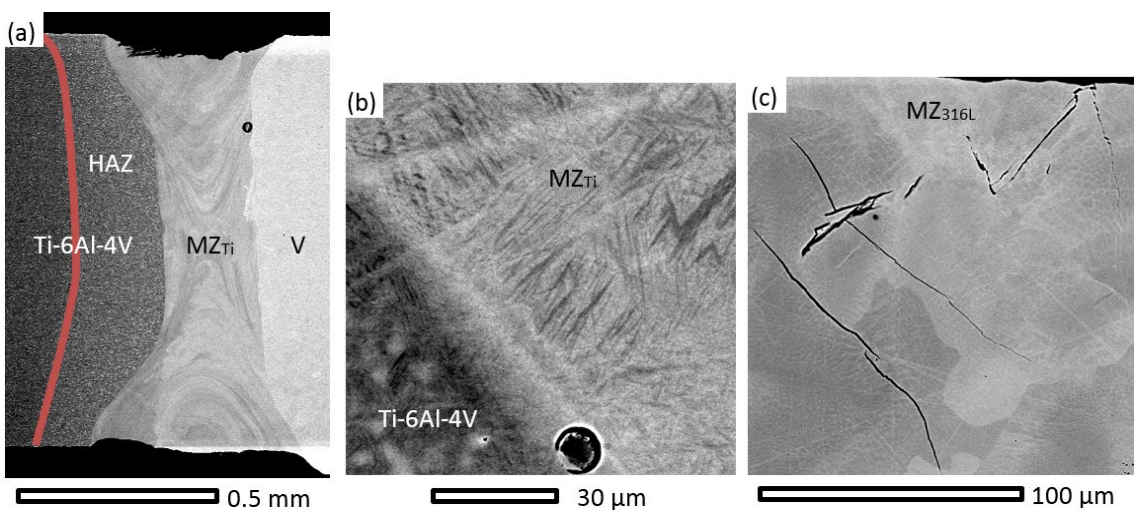

Fig. 2. (a) Ti-6Al-4V/V melted zone (sample b4) with 41 at.% V; (b) Martensitic structure in MZ_{Ti}, for 11 at.% V (sample a8); (c) Cracks of sample b1, on 316L/V melted zone, with 55 at.% V.

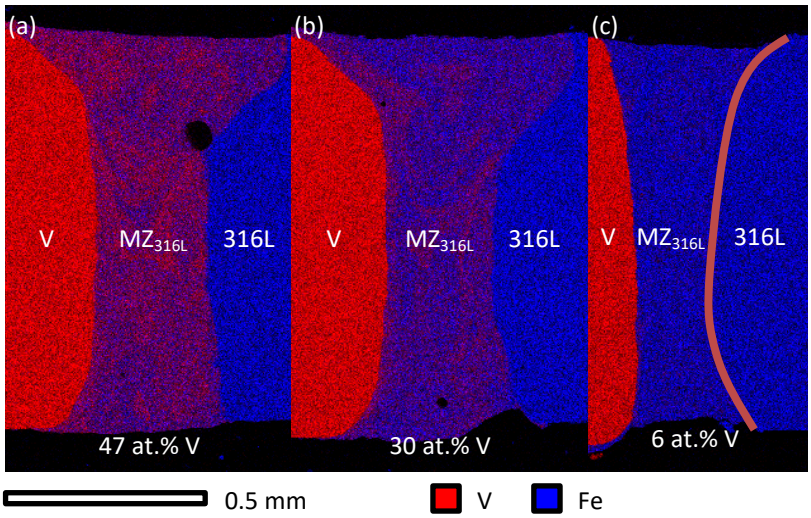

Fig. 3. EDS maps of composition with 100 µm spot and for beam offsets of a) 50 µm to V (sample b1), b) 0 µ m (sample b4), c) 50 µm to 316L (sample b6).

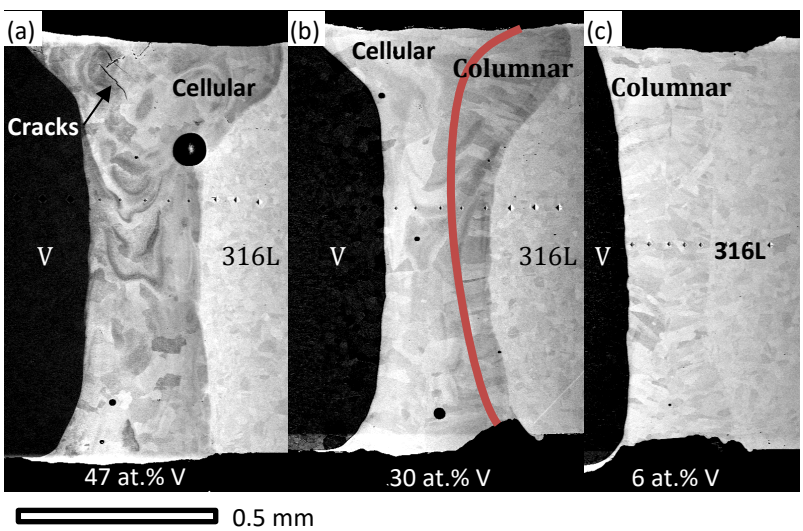

Fig. 4. MZ_{Ti} BSE images with 100 µm spot and for beam offsets of (a) 50µm to V (sample b1); (b) 0 µm (sample b4); (c) 50 µm to 316L (sample b6).

3.2. Hardness measurements

The hardness tests were made approximately at the middle height of the samples (Fig. 4). Fig. 5 represents typical profile of the samples, with hardness around 340 HV for base Ti-6Al-4V, and 200 HV for base 316L. Heat affected zone of Ti-6Al-4V is harder, around 400 HV, possibly due to martensitic transformation. Vanadium hardness profile shows annealed zones near to the limits of the melted zones, with hardness below 140, namely 100 HV, when the raw vanadium has about 170 HV.

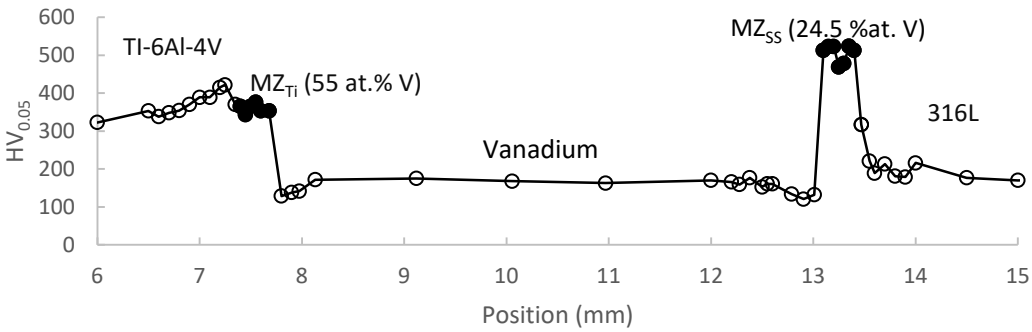

Fig. 5. Typical microhardness profile on the assemblies. Sample a2, welded with 200 µm fiber, 18 J/mm and laser spot offset of 130 µm to V side. Full circles correspond to MZ.

MZ_{Ti} is less hard comparing to the MZ_{316L}. Fig. 6 a shows the hardness dependence on local composition. Under 10 at.% of vanadium, α-Ti and β-Ti phases are thermodynamically stable. Under rapid cooling, a part of β-Ti, stable at high temperature, transforms in martensitic needles (Chu et al. 2017b) shown on Fig. 2 c. This structure is present on the samples welded with offset on Ti-6Al-4V side.

Zhang et al., 2018, detected a metastable ω-Ti phase in Ti/V joints with no beam offset from the joint line, having less than 20 at.% V and average hardness above 470 HV. They considered that the ω phase can appear under 20 at.% V. They measured hardness above 470 HV. The major difference from present study was the use of pulsed laser, leading to more brutal cooling than with continuous laser. Collings, 1975, observed ω-phase formation in quenched alloys of Ti with 13-25 at.% V. ω-Ti is a metastable phase, which can appear with rapid cooling or under high pressures, for metals such as Ti or Zr, enriched with transition metals such as V or Nb. This phase is highly brittle, and is not observable at low magnifications.

Above 10 at.% V, the increase of V content makes little effect on hardness, comprised between 260 and 340 HV.

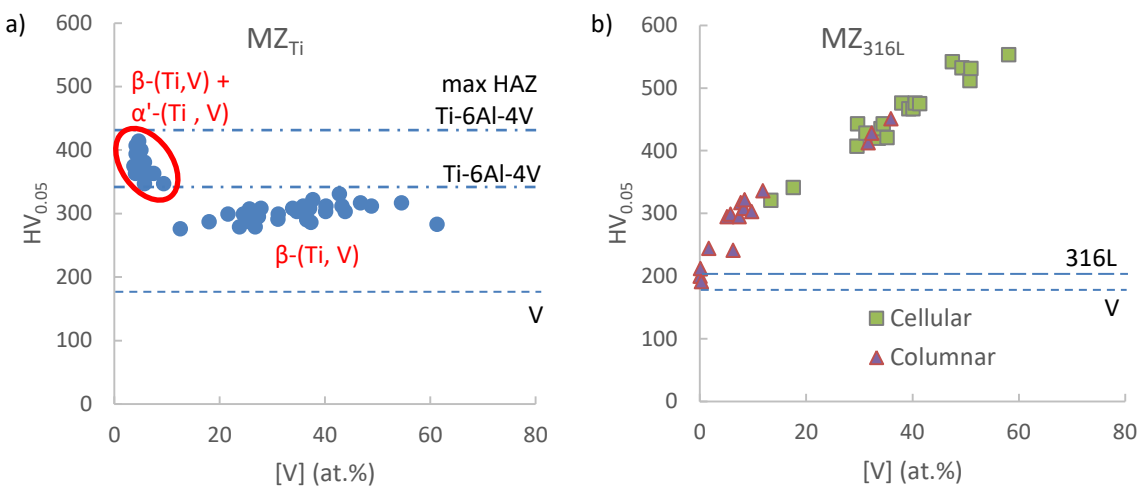

Fig. 6. Local microhardness for the 100 µm spot (a) in MZTi; (b) in MZ316L. The dashed lines indicate the hardness of base metals, the upper line of Ti-6Al-4V corresponds to the higher hardness of HAZ.

MZ_{316L} has much higher hardness (Fig. 6 b). This hardening depends on V content as shown in Fig. 6 b. Already noticeable at 1 at.%, it increases at least to 60 at.% (550 HV). However, according to Nogami et al. 2013 and Adomako et al., 2019, the precipitation of σ-phase, for example after post weld heat treatment, increases the hardness of the MZ up to 1000 HV. Moreover, in several cases, a brittle reactive layer formed at the interface between MZ and V. Therefore, post weld heat treatment is excluded for 316L/V assemblies. The quenching effect avoids σ formation, since σ has a low kinetic of formation. Old binary phase diagrams such (Lyakishev, 1997), did not show that σ is not thermodynamically stable at low temperature. Ustinovshchikov, 2005, observed that under 600 °C, a phase separation occurred at nano scale and produces the hardening of the alloy. The difference of hardness between columnar grains and coarse grains is only caused by their V content, and so, by solution hardening.

3.3. Tensile properties

Fig. 7 and Fig. 8 illustrates typical behavior of Ti-6Al-4V/V/316L joints. Fig. 7 represents the typical tensile curves of the different kinds of fracture observed in this study. Fig. 8 correlates UTS, V content in MZ_{316L} and fracture types. The full forms represent the welds made with 100 µm spot, and empty forms the welds made with 200 µm spot. Fracture types are determined from tensile curves and fractographies (Fig. 9). Curve with diamonds at Fig. 7 corresponds to brittle fracture, observed only in the preliminary experiment, for high V contents, represented by crosses and diamonds on Fig. 8. These fractures occurred in MZ_{316L}, eventually with fracture propagation in ductile V for mixed fractures, right after the end of elastic domain. Unfortunately, higher V contents of 100 µm samples cracked in MZ_{Ti}, due to too important offset to Ti-6Al-4V side (squares on Fig. 8). Cracks brutally occurred at the V/MZ_{Ti} interface, due to lack of vanadium fusion. Then in zones where V melted, the cracks propagated in vanadium with ductile characteristic, creating the step at the terminal part of tensile curve. This type of tensile curve is also observed for too high offsets to 316L side, represented by triangles on Fig. 7 and Fig. 8. Very low V content indicates insufficient V fusion, in other words, a soft brazing. Lower acceptable V content is lower with 100 µm welds than with 200 µm welds. At 5 at.% of V, fracture of 200 µm sample occurred at the interface, while for 100 µm samples, fracture occurred on V HAZ.

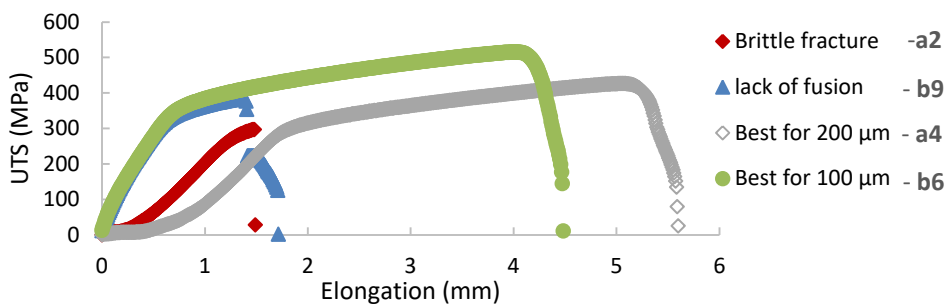

Fig. 7. Tensile curves of different kinds of fracture.

Finally, highest UTS were associated with ductile fractures in vanadium HAZ, represented by circles on Fig. 7 and Fig. 8. In the case of 100 µm spot, these fractures are around the UTS value of raw V. The annealing of V into the second experiment had not a noticeable effect on UTS, but explains why the fractures occurred on HAZ zone. Globally UTS and yield strength of 100 µm spot welds are higher than results of 200 µm spot welds, for a same fracture types. The higher lineic energy with 200 µm spot created wider heat affected zone

in vanadium. A safe zone of MZ_{316L} composition is defined between 10 at.% V and 35 at.% V, when ductile fractures occurred in vanadium.

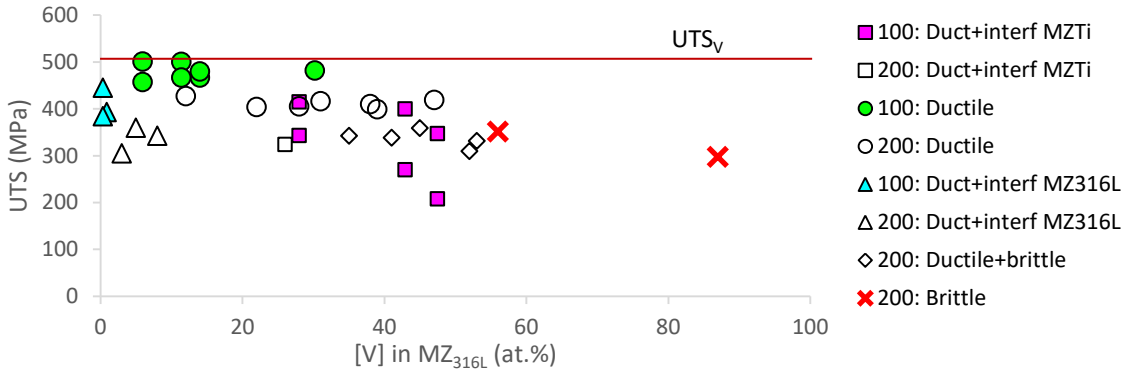

Fig. 8. UTS of samples, correlated with V content in MZ and with fracture kind. Full forms represent results of 100 µm experiment, empty form the results of 200 µm experiment. The line represents our V UTS.

3.4. Fractography

When the V content is too high (> 50 at.% V), the MZ_{316L} became brittle, which is correlated with the increase of hardness. In this case, the fracture shows cleavages, and has the composition identical to the melted zone (Fig. 9 a). In some cases, the fracture initiates in brittle mode, and propagates in V with ductile mode. Optimal MZ_{316L} composition results in ductile fracture in remaining vanadium insert (Fig. 9 b).If beam offset is too high, V does not melt on the full depth, and is only brazed, according to V content on the MZ. The fracture takes place on the V/MZ interface (Fig. 9c), and can propagate on V in ductile mode (Fig. 9 b).

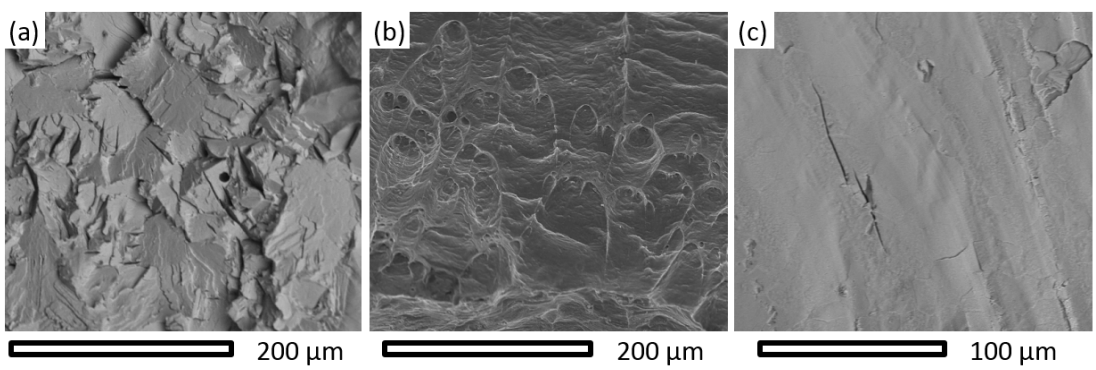

Fig. 9. Fracture surfaces (a) brittle in MZ; (b) ductile in V; (c) interfacial, between V and MZ.

XRD analysis of Fig. 10 a was made on a vanadium-rich fracture (53 at.% V), with coexisting brittle and ductile modes. The sample was weld with the 200 µm spot with no offset. It is one of the best candidates for σ-phase presence. However, σ-phase was not detected, but there were 2 phases, similarly to those observed by Adomako et al., 2019:

- V, which correspond to the ductile propagation on vanadium interlayer. Its intensity is low, because this fracture is mainly brittle than ductile.

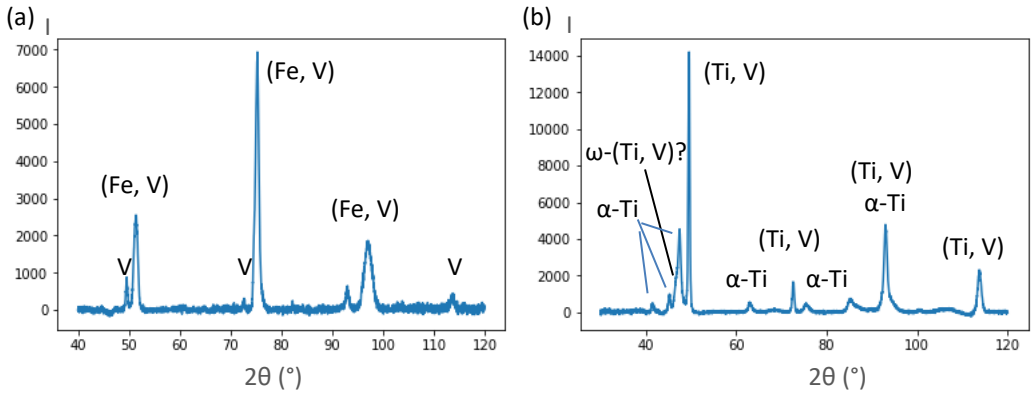

Fig. 10. XRD spectrum of (a) MZ_{316L} brittle and ductile fractured (sample a1) containing 53 at.% V, at 316L side of the fracture; (b) MZ_{Ti} interfacial fractured (sample b3) containing 7 at.% V, at MZ_{Ti} side.

- (Fe,V) is the solid solution of with the same structure than V, but not the different lattice size. It can has the composition of σ-phase that is not found due to the rapid cooling.

Fig. 10 b shows a XRD analysis of an interfacial fracture between MZ_{Ti} and V. It corresponds to the highest hardness measured in MZ_{Ti}. V peaks correspond to the ductile zones, and α-Ti peaks confirm the martensite presence, while for high V contents, phase β-Ti becomes stable. It is not possible to confirm or deny the presence of ω-(Ti, V). It could cause the enlargement of an intense peak of α-Ti, but separate peaks of ω-(Ti, V) are too minor to be distinguished from the noise.

4. Conclusions

Use of vanadium interlayer associated with double pass welding allowed obtaining resistant joints between titanium and stainless steel. The main challenge for this kind of assembly resides in the control of composition of the melted zone involving vanadium and steel. 10-35 at.% V content in MZ_{316L} resulted in resistant melted zones with no embrittlement, and during tensile test purely ductile fracture occurred in unmelted vanadium interlayer. Use of 2 or 6 mm wide interlayer does not influence the final UTS. For the MZ_{316L} with optimum V content, UTS can reach the level of raw vanadium (500 MPa) under condition to minimize the annealing effect in remaining interlayer. Using 100 µm laser spot allows important reduction of heat input and thus is preferential to 200 µm laser spot.

Starting from 35 at.% V MZ_{316L} becomes brittle and risks to develop cold cracking. In absence of σ-(Fe,V), the observed hardening that increases with V content can be attributed to the nano-scale phase separation of (Fe, V) solid solution. The solidification mode MZ_{316L} is also determined by global content of vanadium: coarse cellular microstructure forms in presence of > 40 at.% V and is completely replaced by columnar solidification when V content drops below 10 at.%. Between 10 and 40 at.% V there is a coexistence of cellular and columnar microstructure formed on vanadium and steel side of the melted zone respectively, in spite of quite uniform elements distribution. This evolution of microstructure can be attributed to the different cooling rates on the opposite sides of the weld. The MZ_{316L} containing less than 5 at.% V suffer from lack of fusion, due to excessive beam offset. In this case, featureless fracture associated with low UTS develops in the MZ/V interface.

The melted zone between vanadium and Ti-6Al-4V is rarely a source of problem, because of ideal compatibility between V and Ti, and should be created in the first pass. Excessive offsets from joint line should be avoided to exclude the lack of fusion. Below 10 at.% V, martensitic transformation hardens the

MZ_{Ti} up to the level of HAZ in Ti-6Al-4V, however it does not lead to the embrittlement of the weld. Above 10 at.% V, MZ_{Ti} is composed by solid solution (Ti,V) and its hardness remains below the level of raw Ti-6Al-4V.

Acknowledgements

This work was carried out as a part of joint laboratory project LabCom FLAMme between Laboratoire Interdisciplinaire Carnot de Bourgogne, University of Bourgogne-Franche-Comté and SME Laser Rhône-Alpes. This project was funded by French National Agency of Research.

References

Adomako, N. K., Kim, J. O., Lee, S. H., Noh, K.-O., Kim, J. H., 2018. Dissimilar welding between Ti–6Al–4V and 17-4PH stainless steel using a vanadium interlayer. Materials Science & Engineering A 732, p. 378.

Adomako, N. K., Kim, J. O., & Kim, J. H., 2019. Microstructural evolution and mechanical properties of laser beam welded joints between pure V and 17-4PH stainless steel. Materials Science and Engineering: A 753, p. 208.

Chu, Q., Zhang, M., Li, J., Yan, C., 2017a. Experimental and numerical investigation of microstructure and mechanical behavior of titanium/steel interfaces prepared by explosive welding. Materials Science & Engineering A 689, p. 323.

Chu, Q., Zhang, M., Li, J., Yan, C., Qin, Z., 2017b. Influence of vanadium filler on the properties of titanium and steel TIG welded joints. Journal of Materials Processing Technology 240, p. 293

Collings, E. W., 1975. Magnetic studies of omega-phase precipitation and aging in titanium-vanadium alloys. Journal of the Less Common Metals, 39(1), p. 63.

Dey, H.C., Ashfaq, M., Bhaduri, A.K., Prasad Rao, K., 2009. Joining of titanium to 304L stainless steel by friction welding. Journal of Materials Processing Technology 209, p. 5862.

Fazel-Najafabadi, M., Kashani-Bozorg, S.F., Zarei-Hanzaki, A., 2010. Joining of CP-Ti to 304 stainless steel using friction stir welding technique. Materials and Design 31, p. 4800.

Gloc, M., Wachowski, M., Plocinski, T., Kurzydlowski, K. J., 2016. Microstructural and microanalysis investigations of bond titanium grade1/low alloy steel st52-3N obtained by explosive welding. Journal of Alloys and Compounds 671, p. 446.

Ivanchenko, V., Pryadko, T., 2008, Chromium–Iron–Titanium, In "Ternary Alloy Systems". Springer, Berlin, Heidelberg, p. 365.

Kimura, M., Iijima, T., Kusaka, M., Kaizu, K., & Fuji, A., 2016. Joining phenomena and tensile strength of friction welded joint between Ti–6Al–4V titanium alloy and low carbon steel. Journal of Manufacturing Processes, 24, p. 203.

Liao, J., Yamamoto, N., Liu, H., Nakata, K., 2010. Microstructure at friction stir lap joint interface of pure titanium and steel. Materials Letters 64, p. 2317

Limura, M., Iijima, T., Kusaka, M., Kaizu, K., Fuji, A., 2016. Joining phenomena and tensile strength of friction welded joint between Ti–6Al–4V titanium alloy and low carbon steel, Journal of Manufacturing Processes 24, p. 203.

Lyakishev, N. P, 1997. Spravochnik Diagrammy sostoyania dvoynyh metallicheskih sistem, Mashinostroenie, Moscow, Russian Federation.

Mannucci, A., Tomashchuk, I., Mathieu, A., Cicala, E., Boucheron, T., Bolot, R., Lafaye, S., 2018. Direct laser welding of pure titanium to austenitic stainless steel. Procedia CIRP 74, p. 485.

Nogami, S., Miyazaki, J., Hasegawa, A., Nagasaka, T. , Muroga, T., 2013. Study on electron beam weld joints between pure vanadium and SUS316L stainless steel. Journal of Nuclear Materials 442, p. S562.

Shida, K., Gao, Y., Nagatsuka, K., Takahashi, M., Nakata, K., 2015. Microstructures and mechanical properties of friction stir welded lap joints of commercially pure titanium and 304 stainless steel. Journal of Alloys and Compounds 630, p. 172.

Tomashchuk, I., Grevey, D.,Sallamand, P., 2015. Dissimilar laser welding of AISI 316L stainless steel to Ti6–Al4–6V alloy via pure vanadium interlayer. Materials Science & Engineering A 622, p. 37.

Tomashchuk, I., & Sallamand, P., 2018. Metallurgical strategies for the joining of titanium alloys with steels. Advanced Engineering Materials, 20(6), p. 1700764.

Ustinovshchikov, Y. I., Pushkarev, B. E., Sapegina, I. V., 2005. Mechanism of sigma-phase formation in the Fe-V system. Inorganic materials, 41(8), p. 822.

Zhang, Y., Sun, D., Gu, X., Li, H., 2018. Microstructure and mechanical property improvement of dissimilar metal joints for TC4 Ti alloy to 301L stainless steel. Journal of materials science, 53(4), p. 2942.